J. Biochem. 132, 177–182 (2002)

Solution Structure of a SRP19 Binding Domain in Human SRP RNA[1]

Taiichi Sakamoto,[*] Satoshi Morita,[*] Kazutoshi Tabata,[*] Kouji Nakamura,[†] and Gota Kawai[*,‡,2]

[*]*Department of Industrial Chemistry, Faculty of Engineering, Chiba Institute of Technology, Narashino-shi, Chiba 275-0016;* [†]*Institute of Biological Sciences, University of Tsukuba, Tsukuba-shi, Ibaraki 305-8572; and* [‡]*Genomic Sciences Center, RIKEN Yokohama Institute, Tsurumi-ku, Yokohama 230-0045*

Received April 17, 2002; accepted May 11, 2002

Assembly of the human signal recognition particle (SRP) requires SRP19 protein to bind to helices 6 and 8 of SRP RNA. In the present study, structure of a 29-mer RNA composing the SRP19 binding site in helix 6 was determined by NMR spectroscopy. The two A:C mismatches were continuously stacked to each other and formed wobble type A:C base pairs. The GGAG tetraloop in helix 6 was found to adopt a similar conformation to that of GNRA tetraloop, suggesting that these tetraloops are included in an extensive new motif GNRR. Compared with the crystal structure of helix 6 in complex with SRP19 determined previously, the GGAG tetraloop in the complex was found to adopt a similar conformation to the free form, although the loop structure becomes more open upon SRP19 binding. Thus, SRP19 is thought to recognize the overall fold of the GGAG loop.

Key words: GNAR motif, helix 6, NMR, signal recognition particle, tetraloop.

The signal recognition particle (SRP) plays an important role in the co-translational translocation of secretory proteins across the endoplasmic reticulum (ER) membrane (*1*). Human SRP contains a SRP RNA (300 nucleotides, Fig. 1A) and six proteins (SRP9/14, SRP19, SRP54, and SRP68/72), and is comprised of two domains: *Alu* and large subunits, SRP9/14 heterodimer and half of the SRP RNA form the *Alu* subunit, whereas SRP19, SRP54, SRP68/72 heterodimer, and the other half of the RNA form the large subunit. The consensus secondary structure of the SRP RNA from *Eukarya* and *Archaea* contains six helical domains (helix 2–6 and 8). In contrast, most of the bacterial SRP RNAs consist of only a single helical domain (helix 8), which contains the most conserved regions of SRP RNA. Although SRP-mediated protein translocation occurs by binding of SRP54 to the signal sequences of nascent polypeptides on the ribosome, prior binding of SRP19 to helices 6 and 8 in the large subunit is required for further assembly of SRP54 with the helix 8 in the case of human (*2, 3*). In contrast, bacterial SRP54 homologue (fifty-four homologue, *ffh*) can bind either bacterial or human SRP RNA, and SRP54 from *Archaea* can bind to archaeal SRP RNA (with reduced efficiency) in the absence of SRP19 (*4, 5*). The molecular mechanism for the requirement of SRP19 for the assembly of SRP in *Eukarya* is not clear.

Recent structural characterizations of SRP by X-ray crystallography and NMR spectroscopy have enhanced our understanding of protein–RNA interactions at the atomic level; *Alu* domain (*6, 7*), *ffh* (*8*), helix 8 (*9–11*), complex of helix 8 and M-domain of *ffh* (*12*), SRP19 (*13*), complex of helix 6 and SRP19 (*14*). The crystal structure of SRP19-helix 6 complex revealed that the protein-RNA interactions are mediated by the specific recognition of a widened major groove and the tetraloop without any direct protein-base contacts (*14*). On the other hand, biochemical studies based on mutagenesis and footprinting revealed that a GGAG tetraloop is important for SRP19 binding (*15, 16*). Here, we present the NMR structure of a 29-mer RNA (HE6) comprising the central and distal stem of helix 6, representing the major binding site of SRP19 (Fig. 1B). Our results provide evidence for a structural motif, GNRR motif, and further information about SRP19–helix 6 interaction in assembly of human signal recognition particle.

MATERIALS AND METHODS

RNA Synthesis and Purification—The unlabeled and ^{13}C, ^{15}N-labeled HE6 RNAs were synthesized by *in vitro* transcription reaction using T7 RNA polymerase and purified by PAGE under denaturing conditions as described earlier (*17*). To inprove the resolution of NMR signals, semi-selective [^{13}C,^{15}N]labeling was introduced to A and C, G and U, or G and C using [*U*-^{13}C,^{15}N]NTPs (Nippon Sanso). RNA samples were dissolved in 20 mM sodium phosphate buffer (pH 6.5) containing 50 mM NaCl. Sample concentrations were 0.5 mM. Finally, the samples were annealed by heating at 90°C for 5 min and snap-cooling on ice. To confirm the hairpin structure, the samples were subjected to native

[1]This work was supported by "Research for the Future" Program (JSPS-RFTF97L00503) from the Japan Society for the Promotion of Science. The coordinates have been deposited in the Protein Data Bank (accession number 1L1W). The chemical shift data have been deposited in BioMagResBank (accession number 5321).

[2]To whom correspondence should be addressed. Department of Industrial Chemistry, Chiba Institute of Technology, 2-17-1 Tsudanuma, Narashino-shi, Chiba 275-0016. Phone/Fax: +81-47-478-0425, E-mail: gkawai@ic.it-chiba.ac.jp

Abbreviations: 2D, two-dimensional; COSY, correlated spectroscopy; DQF-COSY, double quantum filtered COSY; ER, endoplasmic reticulum; ffh, fifty-four homologue; HE6, 29-mer RNA fragment in helix 6; HSQC, heteronuclear single-quantum coherence spectroscopy; NOE, nuclear Overhauser effect; NOESY, NOE spectroscopy; SRP, signal recognition particle; TOCSY, total correlation spectroscopy.

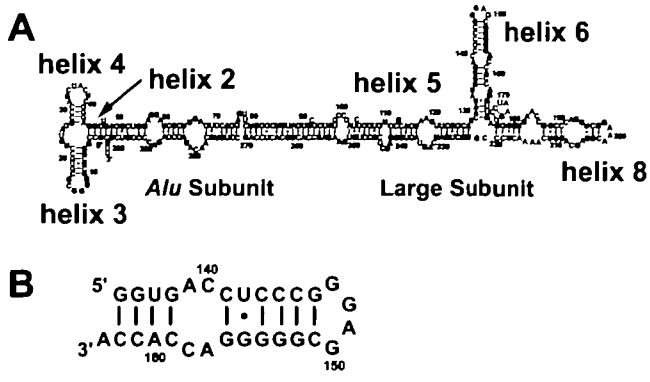

Fig. 1. **A: Secondary structure of human SRP RNA. B: Secondary structure of HE6 (29-mer) used in the present NMR structure determination.**

PAGE analysis before and after NMR experiments.

Analysis of NMR Spectra—Most NMR spectra were measured on a Bruker DRX-600 spectrometer. Some experiments were performed on a Varian Unity-INOVA 800 MHz spectrometer. Spectra were recorded at 7–30°C and NMR data at 25°C were used for structure calculation. Resonance assignments followed well-established procedures (*18*). 2D HNN-COSY experiments were employed to establish base pairing scheme (*19*). 2D HCCH-COSY and 2D HCCH-TOCSY experiments were used to assign sugar spin systems (*20*), while through-backbone assignments were made with 2D HP-COSY experiments (*21*). H2 protons of adenosine were assigned using 2D HCCH-TOCSY experiment and 2D HSQC (*22*). NOE distance restraints from non-exchangeable protons were obtained from 2D NOESY experiments (mixing times of 100 and 400 ms) in D_2O (*23*). Exchangeable proton NOEs were determined by 2D NOESY in H_2O with mixing time of 150 ms using the jump-and-return scheme and gradient pulses for water suppression. Dihedral restraints were obtained from 2D TOCSY, 2D DQF-COSY, and 2D HP-COSY experiments, as described below.

NOE intensities from exchangeable protons were interpreted as distances of 0–3.5 Å (strong) or 0–6 Å (weak), while NOE intensities from non-exchangeable protons were interpreted as distances of 0–3 Å (strong), 0–4 Å (medium), 0–5 Å (weak), or 0–7 Å (very weak). In order to estimate the δ (C5′-C4′-C3′-O3′) dihedral angle, sugar pucker was analyzed using 2D TOCSY and 2D DQF-COSY spectra. A large $^3J_{H1'-H2'}$ coupling constant and a small $^3J_{H3'-H4'}$ coupling constant indicate the C2′-*endo* conformation (δ = 160° ± 30°), whereas a small $^3J_{H1'-H2'}$ coupling constant and a large $^3J_{H3'-H4'}$ coupling constant correspond to the C3′-*endo* conformation (δ = 85° ± 30°). Restraints for the C3′-*endo* conformation were used for G136–C145 and G153–C162, a restraint for the C2′-*endo* conformation was used for G148, and no δ angle restraint was used for other nucleotides. Hydrogen bonding restraints for Watson-Crick base pairs were introduced as distance restraints between proton and heavy atom (1.8–2.5 Å). Forty-four restraints (>5 Å) were added to the distance restraints described above based on the absence of NOE cross peaks.

Structure Calculation—A set of 100 structures was calculated using a simulated annealing protocol with the InsightII/Discover package. The amber force field was used. A total of 375 NOE distance restraints, 102 dihedral restraints, and 28 hydrogen bonding restraints were used. The force constants were 50 kcal mol^{-1} $Å^{-2}$ for distance restraints and 120 kcal mol^{-1} rad^{-2} for dihedral restraints. For randomization of the starting structure, the structures were heated to 1,000 K during 5 ps and cooled to 300 K during another 5 ps, keeping the covalent structure close to being ideally satisfied. The randomized structures were heated to 1,000 K during 5 ps. Distance and dihedral restraints were gradually scaled to full value during 15 ps of molecular dynamics, while maintaining low value for interatomic repulsion, which was subsequently increased to full value during another 20 ps of dynamics. Then, the temperature was gradually scaled to 300 K during 10 ps. A final minimization step was performed, which included a Lennard-Jones potential and electrostatic terms with a dielectric constant of 7. The structures were further refined through a second simulated annealing protocol. After the structure was heated to 1,000 K during 10 ps, all restraints and the interatomic repulsion energy term were rescaled to 1/10 of full value. All restraints were gradually scaled to full value during 5 ps of molecular dynamics, while maintaining low value for interatomic repulsion, which was subsequently increased to full value during another 5 ps of dynamics. An additional 5 ps of dynamics was performed at 1,000 K, and the temperature was gradually scaled to 300 K during 10 ps. A final minimization step was performed, which included a Lennard-Jones potential and electrostatic terms with a dielectric constant of 7. The 15 final structures that had the lowest total energy were chosen.

RESULTS AND DISCUSSION

Structure Determination—The NMR signals were assigned using the standard method involving heteronuclear experiments (Fig. 2A) (*18*). Several unusual protons and ^{31}P chemical shifts were observed in the GGAG loop. H1′ signal of C151 was observed at 5.05 ppm at 25°C, which was shifted upfield (4.89 ppm) at 20°C. G147–G148 and G150–C151 phosphate groups have ^{31}P signals that are shifted downfield (–0.60 and –0.66 ppm respectively) compared to the envelope of A-form phosphorus chemical shifts. Absence of crosspeaks between H1′–H2′ in 2D TOCSY (*24*) and 2D DQF-COSY (*25*) experiments implied that the nucleotides in the stem and the A:C mismatches were in the C3′-*endo* conformations. For the GGAG loop, G148 was found to predominantly be in the C2′-*endo* conformation, A149 and G150 were in equilibrium between the C2′-*endo* and C3′-*endo* conformations, as estimated based on $^3J_{H1'-H2'}$ and $^3J_{H3'-H4'}$ as described previously (*26*). Several broadened signals (for example, H8 and H1′ protons of G147and H1′ proton of C151) indicate conformational flexibility in the loop.

One amino proton signal of G147 could be observed, which was assigned to an intra-residue NOE between the amino proton and imino proton of G147, although signals of guanosine amino protons are generally difficult to observe. This observation is possibly caused by slow-exchange of the amino proton with solvent protons. Furthermore, a strong NOE crosspeak between an amino proton of G147 and H8 proton of G150 was observed (Fig. 2B).

The structure of HE6 was determined using the standard method (*18*). A total of 375 NOE and 102 dihedral

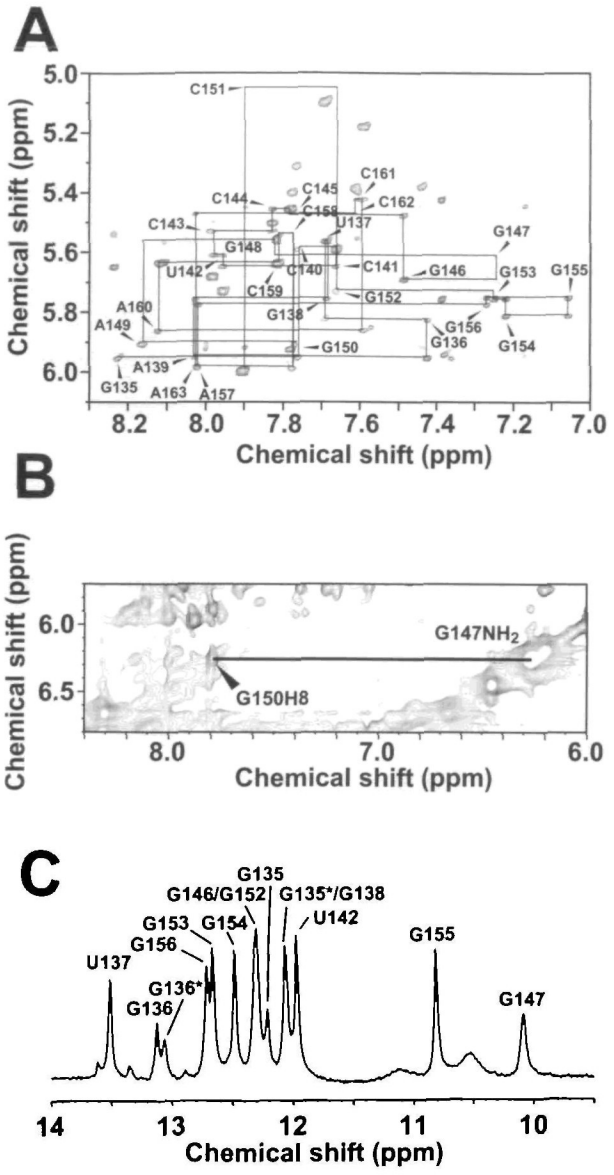

Fig. 2. **NMR spectra of HE6.** A: 2D NOESY spectrum in D_2O (mixing time = 100 ms) at 25°C showing cross-peaks between aromatic H6 and H8 protons and ribose H1′ protons. Sequential connectivities are indicated by lines and intra-residue NOEs are labeled by residues. B: 2D NOESY spectrum in H_2O (mixing time = 150 ms) at 25°C. Resonance of G150 amino proton is marked as a horizontal line. Related NOE cross-peaks are labeled with the name of the connected proton. C: NMR spectrum of exchangeable protons at 7°C. Imino proton assignments are denoted with residue numbers. G135* and G136* indicate peaks due to an RNA that contains extranucleotides at the 3′ terminus, which is the by-product of *in vitro* transcription.

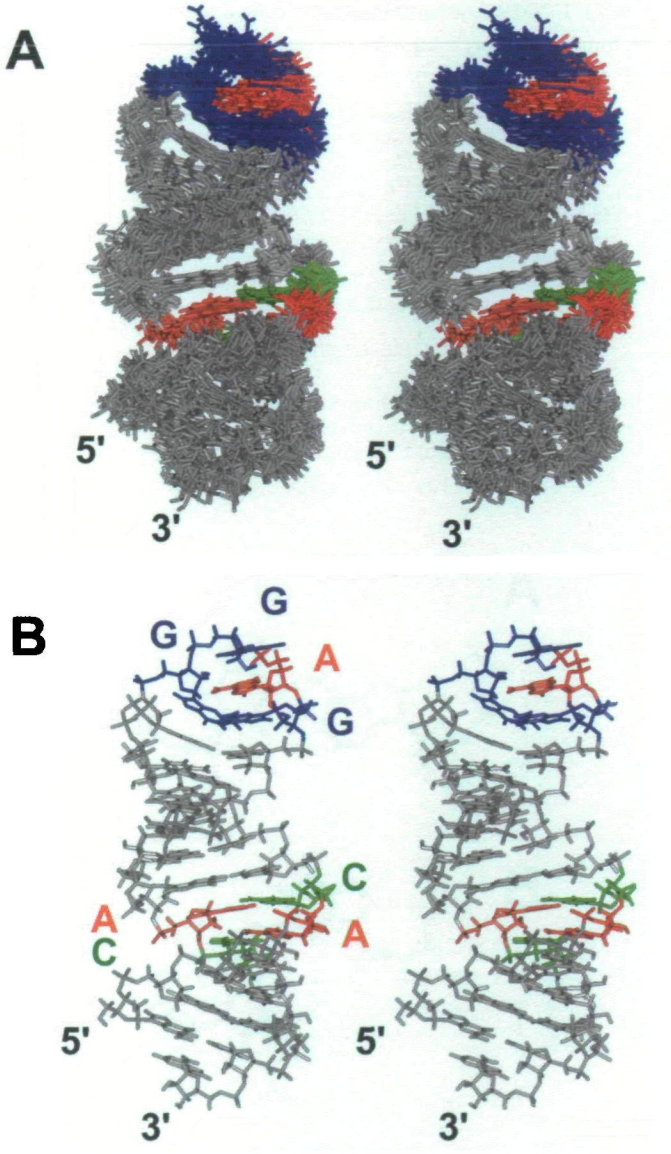

Fig. 3. **Tertiary structures of HE6 solved by NMR.** A: Stereo view of the superposition of final 15 structures of HE6. G, A, and C residues in the GGAG loop and the A:C mismatches are colored in blue, red, and green, respectively. B: Stereo view of the minimized average structure of HE6.

angle restraints were obtained from NMR data. Structures were calculated using restrained molecular dynamics in a simulated annealing protocol. A total of 15 structures converged to low total energy (Fig. 3). The overall structure is well defined by the NMR data with a heavy atom root-mean-square deviation (r.m.s.d.) for the 15 structures of 1.18 Å (Table I).

Structure of Tandem A:C Mismatches—The local structure of the non-canonical 5′-AC-3′/3′-CA-5′ tandem mismatches separating the two helical regions was well defined in the calculated structure of HE6 (heavy atoms r.m.s.d. was 0.67 Å). The structure shows that the bases in 5′-GACC-3′/3′-CCAG-5′ (138–141 and 156–159) are continuously stacked, which is consistent with sequential interbase NOEs and NOE connectivity for H2(A139)–H1′(C140), H2(A139)–H1′(C159), H2(A157)–H1′(C158), H2(A157)–H1′(C141). Wobble type A:C base pairs were formed in the calculated structure (Fig. 4A), although direct evidence for the A:C base pair formation could not be observed in NMR study.

The structure of helix 6 in the duplex form was characterized by X-ray crystallography in the previous study (*27*). Two conformations of wobble type A:C base pairs were formed in the crystal structure because of different protonation states at the adenosine N1 position. The structure of

TABLE I. **NMR restraints and structural statistics.**

Number of experimental restraints	
Distance restraints	375
Dihedral restraints	102
Hydrogen bonding distance restraints	28
r.m.s. deviation from restraints	
Distance restraints (Å)	0.015 ± 0.002
Dihedral restraints (°)	0.2 ± 0.3
r.m.s. deviation from idealized geometry	
Bonds (Å)	0.0029 ± 0.0001
Angle (°)	0.63 ± 0.01
Impropers (°)	0.46 ± 0.01
Heavy-atoms r.m.s. deviation (Å)[a]	
All	1.18
A:C (G138–C141, G156–C159)	0.61
Loop (G146–C151)	1.10

[a]Averaged r.m.s.d. between an average structure and the 15 converged structures were calculated. The converged structures did not contain experimental distance violation of >0.2 Å or dihedral violation >5°.

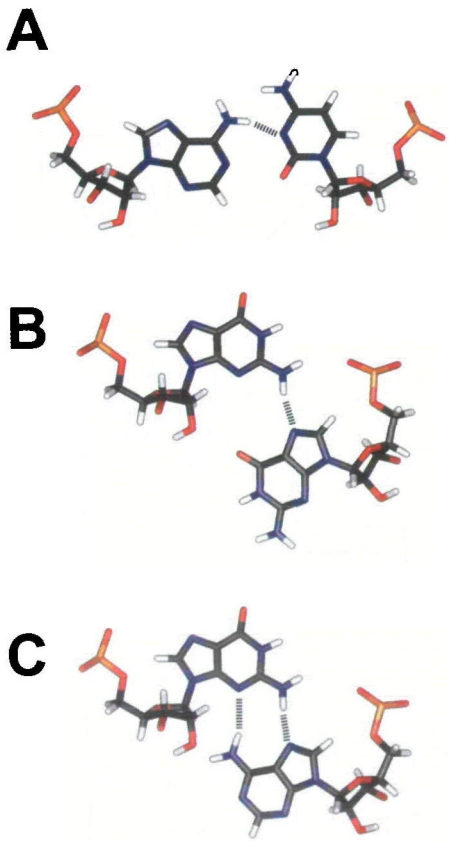

Fig. 4. **Schematic representation of non-canonical base pairs.** Hydrogen bonds are indicated by dotted lines. A: A:C base pair in the present structure (A139:C158). The structures of the two A:C pairs are almost identical (heavy atoms r.m.s.d. was 0.63 Å). B: G:G base pair in the present structure. C: G:A base pair in the GNRA structure.

the A:C base pairs in helix 6 determined in the present study is similar to those determined by X-ray crystallography (heavy atoms r.m.s.d. of 5′-GACC-3′/3′-CCAG-5′ were 0.90 and 0.91 Å). Furthermore, the structure of the A:C base pairs in the free helix 6 determined in the present NMR study is similar to that in the complex determined by

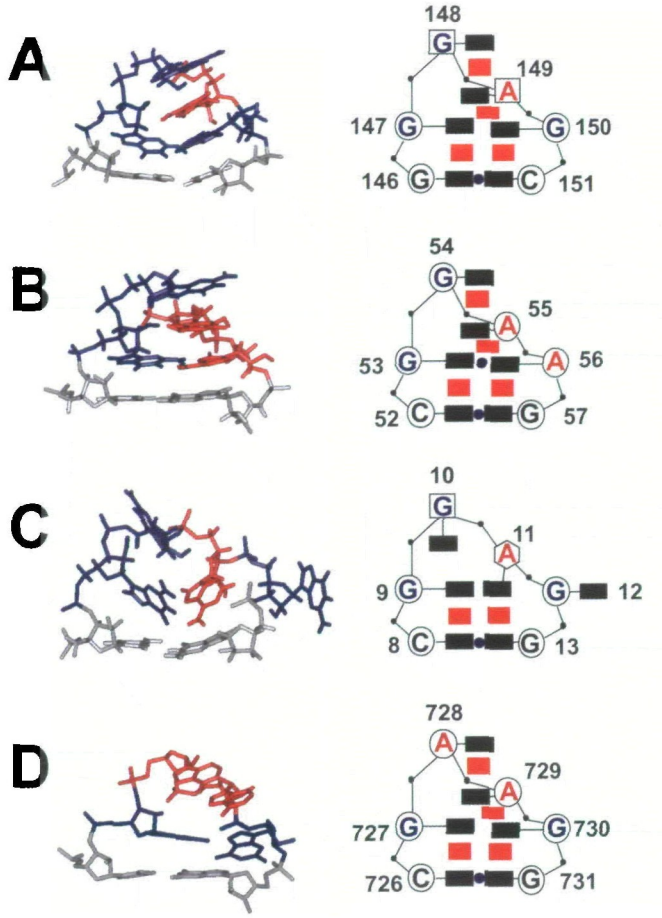

Fig. 5. **Comparison of purine-rich tetraloop structures and its schematic representation.** Original residue numbers are shown. The following symbols are used in the schematic representation: black rectangle, base; red rectangle, stacking interaction; blue circle, hydrogen bonding interaction; open circle, C3′-*endo* ribose; open square, C2′-*endo* ribose; open hexagon, intermediate between C3′-*endo* and C2′-*endo* (O4′-*endo* ribose). A: The GGAG loop structure in helix 6 (in the present structure). B: The GGAA loop structure in *E. coli* SRP RNA (*9*). C: The GGAG loop structure in SL3 of HIV-1 (*29*). D: The GAAG loop structure in helix 23a of 16S rRNA (S15, S6, S18-rRNA complex) (*32*).

X-ray crystallography (Heavy atoms r.m.s.d. was 0.76 Å) (*14*). Thus, the structure of the tandem A:C base pairs is supposed not to be changed upon SRP19 binding.

Structure of GGAG Loop—The local structure of the GGAG loop (G146–C151) is well defined in the calculated structure of HE6 (Fig. 5A, heavy atoms r.m.s.d. was 0.94 Å), although conformation for the glycosidic bond (χ angle) of G148 is not defined. In fact, strong intra-residue NOEs for both H8–H1′ and H8–H2′ in G148 were observed, indicating the rotation around the glycosidic bond. In contrast, the heavy atoms r.m.s.d. for G146–C151 except the G148 base was 0.63 Å. G147 is stacked on G146, and a sharp turn in the phosphodiester backbone occurs between G147 and G148. The three nucleotides A149–C151 are continuously stacked, and this is consistent with the NOE connectivity for H8(G150)–H1′(C151), H8(G150)–H6(C151), H8(G150)–H5(C151), H8(A149)–H8(G150). Furthermore, an NOE between H8(G148) and H8(A149) indicated the existence of stacking between G148 and A149 in a significant popula-

tion. The structure qualitatively explains the unusual chemical shifts observed in the loop. The H1′ signal of C151 is shifted downfield slightly by the ring current of the guanosine base in G150. The downfield ^{31}P signals are consistent with the unusual backbone geometry in the loop. The structure of the GGAG loop in HE6 is similar to the well-characterized GNRA loop structure (*9, 28*) (Fig. 5B), although sugar conformations of G148 and A149 are different from those in the GNRA loop. To explain the reason why second G and third A in GGAG loop have a preference for the C2′-*endo* conformation, further investigation is required.

The calculated structures reveals that G147 and G150 form a sheared type G:G base pair, which is similar to the G:A base pair in the GNRA loop (Fig. 4, B and C). Formation of the G:G base pair is consistent with a strong NOE cross-peak between amino proton of G147 and H8 proton of G150 (Fig. 2B). The HNN-COSY experiment (*19*) optimized for the amino proton might give further evidence for the G:G base pair formation. Upfield-shifted resonance (at approximately 10 ppm) of the imino proton of G:A base pair in the GNRA loop was observed in the previous NMR study of GNRA loop (*9, 28, 29*). Similar resonance of the imino proton of G147 was observed at 10.09 ppm in this study (Fig. 2C). Furthermore, the G:G base pair is thought to be less stable than the G:A base pair, which is consistent with the conformational flexibility of the GGAG loop indicated by some broadening of NMR signals.

Another GGAG loop structure was previously presented (*30, 31*) in the SL3 stem-loop from HIV-1 that adopts a different fold from that in the present study (Fig. 5C). The characteristic features of the loop structure in SL3 are the unstacked structure of G12 (the fourth nucleotide) and the stacking of A11 upon G13, which is consistent with the non-sequential NOE connectivities for H8(A11)–H1′(G13), H1′(A11)–H1′(G13). In the present study, we could not observe these NOEs. A possible reason for this difference is the difference in the base pair closing the GGAG loop, G:C in the HE6 and C:G in the SL3 stem-loop as shown in Fig. 5, or the conditions for sample preparation or NMR measurement.

Mutagenesis study has revealed that A149 in the GGAG loop is important for the SRP19 binding (*15*). Comparative sequence analysis of SRP RNA showed that the helix 6 tetraloop is represented as a GNAR motif (*32*). In fact, the SRP database shows that the GNAR motif consists of GNAG in 65% and GNAA in 35% of cases, with only a few exceptions for *eukarya* and *archaea* (Signal Recognition Particle Database Web Page by Christian Zwieb, 28 September, 2001, http://psyche.uthct.edu/dbs/SRPDB/SRPDB.html). Thus, the structural motif GNAR must be important for SRP19 binding to helix 6. In addition, GNRA and GNRG could be included in the GNRR motif because of conformational similarity, although the fold of GNRG is more flexible than that of GNRA.

The crystal structure of S15, S6, S18-rRNA complex revealed that the GAAG tetraloop in helix 23a of 16*S* rRNA folds into a GNRA-type conformation (*33*) (Fig. 5D). Although the GAAG loop is not the predominant binding site for S15 protein, the interaction between the third nucleotide adenosine of the loop and the S15 protein was found in the crystal structure. Furthermore, the main alternative of the loop is GAAA, although most of the loop is GAAG. Thus, the structure of the GAAG loop also justifies the GNRR motif.

Comparison of the Free and SRP19-Bound Structures of Helix 6—The crystal structure of the SRP19-helix 6 complex has revealed that SRP19 binds to helix 6 through contact with the phosphodiester backbone of nucleotides C140–C143 and G147–C151 (including the GGAG tetraloop) (*14*). The superimposition of the structures based on the G136–U142 and G155–C161 (heavy atoms r.m.s.d. was 1.06 Å for the region of superimposition and 2.93 Å for G136–C161) revealed that the major groove side of the GGAG loop is widened by the SRP19 binding with the largest movement of 9.1 Å for N6 of A149, while the A:C mismatches are not moved (Fig. 6A). The GGAG loop in the complex adopts a conformation similar to that of free helix 6 but with some differences (Fig. 6B). The GGAG loop in the complex adopts a much more open conformation compared to that of free helix 6. When the G146:C151 base pairs are superposed, it was found that some inserted water molecules displace the last three bases of the loop away from the central axis of the loop, with movements of 5.4 and 4.2 Å for the second and third bases, respectively. Thus, SRP19 distorts the GGAG loop conformation, and the conformational flexibility of the GGAG loop may contribute to the induced fitting upon SRP19 binding.

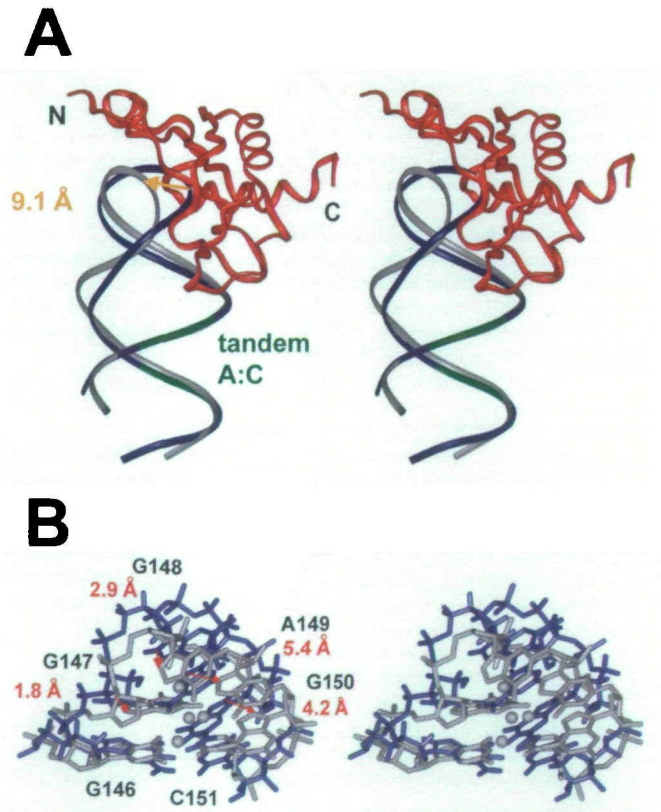

Fig. 6. **Structural changes upon SRP19 binding.** A: The structures of helix 6 in the presence (grey) (*14*) and absence (blue) of SRP19 (red). The superimposition of the structures is based on the nucleotides G136:U142 and G155:C161. B: The structures of the GGAG loop in the presence (grey) (*14*) and absence (blue) of SRP19. Four oxygen atoms of water molecules found in the crystal structure of the complex are represented as gray spheres. The superimposition of the structures is based on the closing base pair G146:C151.

In the case of the GGAG loop of SL3 in HIV-1, the interaction with the nucleocapsid protein leads to complete unstacking of the bases in the loop. The GGAG loop of SL3 does not belong to the GNAR motif, and nucleocapsid protein was shown to interact tightly with the second, third, and fourth bases in a previous NMR study (*34*). In contrast to the case of nucleocapsid protein and SL3 RNA, SRP19 binds mainly to phosphodiester backbone of the GGAG loop. SRP19 is thought to recognize the overall fold of the GGAG loop, that is, the GNAR motif, and causes little change in the loop conformation upon SRP19 binding.

We thank H. Sato, Dr. N. Nemoto, Dr. N. Nameki, A. Takasu, K. Fujiwara, and M. Fujii for technical supports and helpful comments.

REFERENCES

1. Lütcke, H. (1995) Signal recognition particle (SRP), a ubiquitous initiator of protein translocation. *Eur. J. Biochem.* **228**, 531–550
2. Walter, P. and Blobel, G. (1983) Disassembly and reconstitution of signal recognition particle. *Cell* **34**, 525–533
3. Yin. J., Yang, C.-H., and Zwieb, C. (2001) Assembly of the human signal recognition particle (SRP): Overlap of regions required for binding of protein SRP54 and assembly control. *RNA* **7**, 1389–1396
4. Ribes, V., Romisch, K., Giner, A., Dobberstein, B., and Tollervey, D. (1990) *E. coli* 4.5S RNA is part of a ribonucleoprotein particle that has properties related to signal recognition particle. *Cell* **63**, 591–600
5. Diener, J.L. and Wilson, C. (2000) Role of SRP19 in assembly of the *Archaeoglobus fulgidus* signal recoginition particle. *Biochemistry* **39**, 12862–12874
6. Birse, D.E., Kapp, U., Strub, K., Cusack, S., and Aberg, A. (1997) The crystal structure of the signal recognition particle *Alu* RNA binding heterodimer, SRP9/14. *EMBO J.* **16**, 3757–3766
7. Weichenrieder, O., Wild, K., Strub, K., and Cusack, S. (2000) Structure and assenmbly of the *Alu* domain of the mammalian siganl recognition particle. *Nature* **408**, 167–173
8. Keenan, R.J., Freymann, D.M., Walter, P., and Stroud, R.M. (1998) Crystal structure of the signal sequence binding subunit of the signal recognition particle. *Cell* **94**, 181–191
9. Schmitz, U., James, T.L., Lukavsky, P., and Walter, P. (1999) Structure of the most conserved internal loop in SRP RNA. *Nature Struct. Biol.* **6**, 634–638
10. Schmitz, U., Behrens, S., Freymann, D.M., Keenan, R.J., Lukavsky, P., Walter, P., and James, T.L. (1999) Structure of the phylogenetically most conserved domain of SRP RNA. *RNA* **5**, 1419–1429
11. Jovine, L., Hainz, T., Oubridge, C., Scott, W.G., Li, J., Sixma, T.K., Wonacott, A., Skarzynski, T., and Nagai, K. (2000) Crystal structure of the Ffh and EF-G binding sites in the conserved domain IV of *Escherichia coli* 4.5S RNA. *Structure* **8**, 527–540
12. Batey, R.T., Rambo, R.P., Lucast, L., Rha, B., and Doudna, J.A. (2000) Crystal structure of the ribonucleoprotein core of the signal recognition particle. *Science* **287**, 1232–1239
13. Pakhomova, O.N., Deep, S., Huang, Q., Zwieb, C., and Hinck, A.P. (2002) Solution structure of protein SRP19 of *Archaeoglobus fulgidus* signal recognition particle. *J. Mol. Biol.* **317**, 145–158
14. Wild, K., Sinning, I., and Cusack, S. (2001) Crystal structure of an early protein-RNA assembly complex of the signal recognition particle. *Science* **294**, 598–601
15. Zwieb, C. (1992) Recognition of a tetranucleotide loop of signal recognition particle RNA by protein SRP19. *J. Biol. Chem.* **267**, 15650–15656
16. Rose, M.A. and Weeks, K.M. (2001) Visualizing induced fit in early assembly of the human signal recognition particle. *Nat. Struct. Biol.* **8**, 515–520
17. Nakamura, K., Miyamoto, H., Suzuma, S., Sakamoto, T., Kawai, G., and Yamane, K. (2001) Minimal functional structure of *Escherichia coli* 4.5S RNA required for binding EF-G. *J. Biol. Chem.* **276**, 22844–22849
18. Allain, F.H.-T. and Varani, G. (1995) Structure of the P1 helix from group I self-splicing introns. *J. Mol. Biol.* **250**, 333–353
19. Dingley, A.J. and Grzesiek, S. (1998) Direct observation of hydrogen bonds in nucleic acid base pairs by internucleotide $^{2}J_{NN}$ couplings. *J. Am. Chem. Soc.* **120**, 8293–8297
20. Pardi, A. and Nikonowicz, E.P. (1992) Simple procedure for resonance assignment of the sugar protons in ^{13}C labeled RNA. *J. Am. Chem. Soc.* **114**, 9202–9203
21. Sklénar, V., Miyashiro, H., Zon, G., Miles, H.T., and Bax, A. (1986) Assignment of the ^{31}P and ^{1}H resonances in oligonucleotides by two-dimensional NMR spectroscopy. *FEBS Lett.* **208**, 94–98
22. Legault, P., Farmer, B.T. II, Mueller, L., and Pardi, A. (1994) Through-bond correlation of adenine protons in a ^{13}C-labeled ribozyme. *J. Am. Chem. Soc.* **116**, 2203–2204
23. Jeener, J., Meier, B.H., Bachmann, P., and Ernst, R.R. (1979) Investigation of exchange processes by two-dimensional NMR spectroscopy. *J. Phys. Chem.* **71**, 4546–4553
24. Bax, A. and Davis, D.G. (1985) MLEV-17-based 2D homonuclear magnetization transfer spectroscopy. *J. Magn. Reson.* **65**, 355–360
25. Rance, M., Sørensen, O.W., Bodenhausen, G., Wagner, G., Ernst, R.R., and Wüthrich, K. (1983) Improved spectral resolution in COSY NMR spectra of proteins via double quantum filtering. *Biochem. Biophys. Res. Commun.* **117**, 479–485
26. Altona, C. and Sundaralingam, M. (1973) Conformational analysis of the suger ring in nucleotides and nucleosides. Improved method for the Interpretation of proton magnetic resonance coupling constants. *J. Am. Chem. Soc.* **95**, 2333–2344
27. Wild, K., Weichenrieder, O., Leonard, G.A., and Cusack, S. (1999) The 2 Å structure of helix 6 of the human signal recognition particle RNA. *Struct. Fold. Des.* **7**, 1345–1352
28. Jucker, F.M., Heus, H.A., Yip, P.F., Moors, E.H.M., and Pardi, A. (1996) A network of heterogeneous hydrogen bonds in GNRA tetraloops. *J. Mol. Biol.* **264**, 968–980
29. Orita, M., Nishikawa, F., Shimayama, T., Taira, K., Endo, Y., and Nishikawa, S. (1993) High-resolution NMR study of a synthetic oligonucleotide with a tetranucleotide GAGA loop that is a substrate for the cytotoxic protein, ricin. *Nucleic Acids Res.* **21**, 5670–5678
30. Pappalardo, L., Kerwood, D.J., Pelczer, I., and Borer, P.N. (1998) Three-dimensional folding of an RNA hairpin required for packaging HIV-1. *J. Mol. Biol.* **282**, 801–818
31. Zeffman, A., Hassard, S., Varani, G., and Lever, A. (2000) The major HIV-1 packaging signal is an extended bulged stem loop whose structure is altered on interaction with the Gag polyprotein. *J. Mol. Biol.* **297**, 877–893
32. Zwieb, C. (1992) Conformity of RNAs that interact with tetranucleotide loop binding proteins. *Nucleic Acids Res.* **20**, 4397–4400
33. Agalarov, S.C., Prasad, G.S., Funke, P.M., Stout, C.D., and Williamson, J.R. (2000) Structure of the S15, S6, S18-rRNA complex: Assembly of the 30S ribosome central domain. *Science* **288**, 107–112
34. De Guzman, R.N., Wu, Z.R., Stalling, C.C., Pappalardo, L., Borer, P.N., and Summers, M.F. (1998) Structure of the HIV-1 nucleocapsid protein bound to the SL3 Ψ-RNA recognition element. *Science* **279**, 384–388